Chemical Science

ROYAL SOCIETY OF CHEMISTRY

EDGE ARTICLE

View Article Online
View Journal



Check for updates

Cite this: DOI: 10.1039/d5sc03374h

All publication charges for this article have been paid for by the Royal Society of Chemistry

Received 9th May 2025
Accepted 28th June 2025

DOI: 10.1039/d5sc03374h

rsc.li/chemical-science

# Bis(amidophenolate)-supported pnictoranides: Lewis acid-induced electromerism in a bismuth complex†

Simon B. H. Karnbrock,[a] Jan F. Köster,[a] Isabelle Becker,[b] Christopher Golz,[a] Franc Meyer,[b] Martí Gimferrer[c] and Manuel Alcarazo*[a]

The synthesis of the complete series of 10-Pn-4 bis(amidophenolate)-supported pnictoranide anions is reported. Coordination of these anions to the cyclopentadienyliron(II) dicarbonyl fragment, $[CpFe(CO)_2]^+$, delivers the corresponding 10-Pn-5 complexes for P, As and Sb, while in the case of Bi an electron redistribution takes place, and the corresponding 12-Bi-5 compound is isolated. This case of Lewis acid-induced electromerism has been experimentally confirmed through X-ray diffraction analyses as well as IR, UV-Vis and Mössbauer spectroscopy. Effective Oxidation State analysis of the Fe-complexes assigns an oxidation state +3 to all Pn, while it predicts the Fe-atom to be reduced to Fe(0) in the Bi-derivative. The mixture of the Bi(6p) orbital with the π-system of the bis(amidophenolate) ligand and the efficient electronic donation from this orbital to the Fe-center explain this situation.

## Introduction

Electromerism, the process of electron density relocation between redox active sites in a molecule,[1] has evolved from being considered a curiosity to a practical tool for the design of magnetic materials, molecular switches, and even active catalysts (Scheme 1a).[2] These applications rely on the very different physicochemical properties that electromers exhibit, and the nature of the different stimuli that are able to trigger their interconversion; namely, temperature,[3] pressure,[4] light[5] or constitutional changes, such as the coordination to Lewis acids or bases.[6]

Ever since the seminal report by Buchanan and Pierpont on electromerism in a cobalt bis(dioxolene)(bipyridyl) complex,[7] this field of research has mostly been associated with transition metal chemistry.[1] Valence tautomeric p-block element compounds are, in comparison, underrepresented.[8] Seminal examples include Ge(II) tetraphenylporphyrin **A** reported by Vaid, in which Lewis base coordination induces the oxidation of Ge(II) to Ge(IV) with concomitant two-electron reduction of the porphyrin unit to its 20π-electron antiaromatic state (Scheme 1b);[9] and the geometrically constrained P(I)-compound **C**. Interestingly, reaction of **C** with $(cod)PtI_2$ leads to the formation of the corresponding Pt-complex **D**, in which the oxidation of

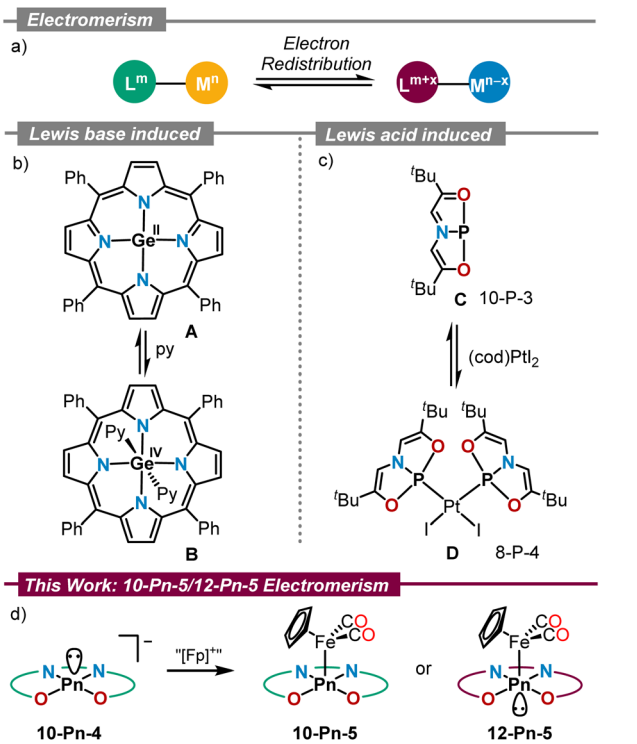


Scheme 1 Electromerism in main group chemistry: (a) concept; (b and c) electromerism induced by coordination to Lewis bases and acids; (d) this work.

[a]Institute of Organic and Biomolecular Chemistry, University of Göttingen, Tammannstraße 2, 37077 Göttingen, Germany. E-mail: manuel.alcarazo@chemie.uni-goettingen.de

[b]Institute of Inorganic Chemistry, University of Göttingen, Tammannstraße 4, 37077 Göttingen, Germany

[c]Institute of Physical Chemistry, University of Göttingen, Tammannstraße 6, 37077 Göttingen, Germany

† Electronic supplementary information (ESI) available. CCDC 2448026–2448035. For ESI and crystallographic data in CIF or other electronic format see DOI: https://doi.org/10.1039/d5sc03374h

the P-center to P(III) has taken place with simultaneous reduction of the supporting ONO scaffold (Scheme 1c).[10] More recently, examples of main group electromerism induced by coordination to Lewis acids or Lewis bases have also been found in Si,[11] Ge,[12] Sn,[13] As[14] and Sb[15] chemistry.

As continuation to our ongoing efforts to understand the redox-activity of pnictogen compounds supported by the rigid tetradentate bis(amidophenolate) ligand **1**,[14,16] we now describe the synthesis and characterization of the complete series of pnictide anions derived from that ligand, compounds **3a–d**, and their corresponding cyclopentadienyliron dicarbonyl complexes **4a–c** and **4d′**. X-ray crystallographic analyses evidence that for all anions **3a–d** the central pnictogen adopts a 10-Pn-4 configuration from which a Pn(III)-oxidation state is inferred. Upon coordination to $[CpFe(CO)_2]^+$ the situation remains identical for the P-, As-, and Sb-complexes **4a–c**, respectively; however, in **4d′** a valence shell expansion from 10-Bi-5 to 12-Bi-5 occurs at the Bi-center. An Effective Oxidation State (EOS) analysis of that complex still assigns an oxidation state +3 to Bi, while the bis(amidophenolate) ligand gets oxidised (−2) and Fe reduced from Fe(II) to Fe(0). Thus, the geometrical rearrangement at Bi serves to better transfer the electron density from the bis(amidophenolate) scaffold to Fe.

## Results and discussion

### Synthesis and structure of 10-Pn-4 anions

Building on our recent studies on bis(amidophenolate)-supported phosphorus and arsenic species **3a,b** (ref. 14 and 16) we started our investigation with the syntheses of their higher Sb- and Bi-analogues **3c** and **3d**, respectively. The necessary stibine precursor **2c** was prepared by reaction of $SbCl_3$ and **1** in the presence of triethylamine; yet, the corresponding bismuthine **2d** was not accessible following that route. Fortunately, compound **2d** could be cleanly prepared by treatment of **1** with $Bi(NMe_2)_3$ at −78 °C in $Et_2O$ (Scheme 2). Deprotonation of **2a–d** was readily achieved by treatment with potassium hexamethyldisilazide (KHMDS) in $Et_2O$ employing [2.2.2]cryptand to sequester the potassium cation. Compounds **3a–d** precipitate from the reaction mixture, and are obtained in analytically pure form by subsequent washing and drying. Quality crystals for X-ray diffraction analysis were obtained by slowly cooling saturated solutions of **3a–d** in an appropriate solvent (see ESI†).

Interestingly, **3a** was found to crystallize as two polymorphs. The first one crystallizes in the hexagonal space group $P6_1$ and features a directed interaction between the phosphorus donor atom and the potassium cation. The P1–K1 distance was determined to be 4.3934(13) Å, and is slightly shorter than the sum of van-der-Waals radii (4.55 Å).[17] The second polymorph, which crystallizes in the monoclinic space group $P2_1/c$, does not feature this interaction (shortest P1–K1 distance: 7.669(3) Å) and is, therefore, better suited for a geometric comparison. In all the higher homologues **3b–d**, the ions were also found to be well separated. All 10-Pn-4 anions **3a–d** exhibit a geometry between square pyramidal and disphenoidal around the central pnictogen due to the geometric constraint imposed by the tetradentate bis(amidophenolate) scaffold and the lower tendency to hybridize of the orbitals of heavier atoms. The difference in the *trans* basal angles $\Delta\theta$ around the pnictogen center has been used as quantitative parameter to illustrate the geometric change (Fig. 1a). As expected, the heavier homologues get closer to an ideal square pyramid (**3c:** $\Delta\theta = 4.3°$, **3d:** $\Delta\theta = 5.2°$ (average value)), while for the lighter congeners the disphenoidal arrangement becomes more favorable (**3a:** $\Delta\theta = 44.8°$, **3b:** $\Delta\theta = 35.5°$) (Fig. 1b). Despite of this, the energetic landscape connecting these structures seems to be rather flat and strongly

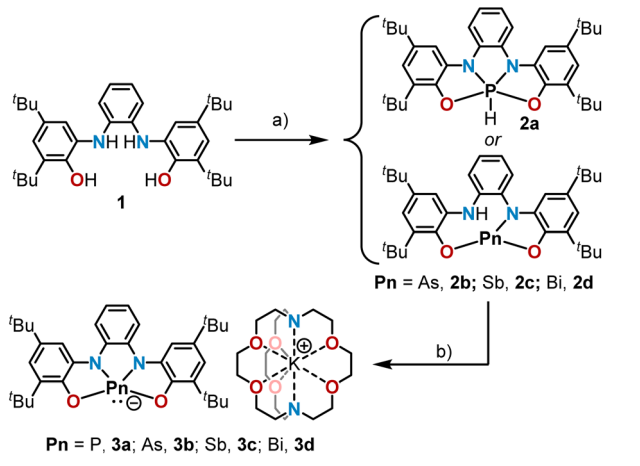


Scheme 2 Synthesis of **3a–d**. (a) **2a**: $PCl_3$ (1.05 equiv.), DIPEA (3.15 equiv.) (54%); **2b**: $AsCl_3$ (1.00 equiv.), $NEt_3$ (3.00 equiv.) (96%); **2c**: $SbCl_3$ (1.00 equiv.), $NEt_3$ (3.00 equiv.) (94%); **2d**: $Bi(NMe_2)_3$ (1.00 equiv.) (89%). (b) KHMDS (1.00 equiv.), cryptand (1.00 equiv.) **3a** (81%), **3b** (89%), **3c** (92%), **3d** (88%).

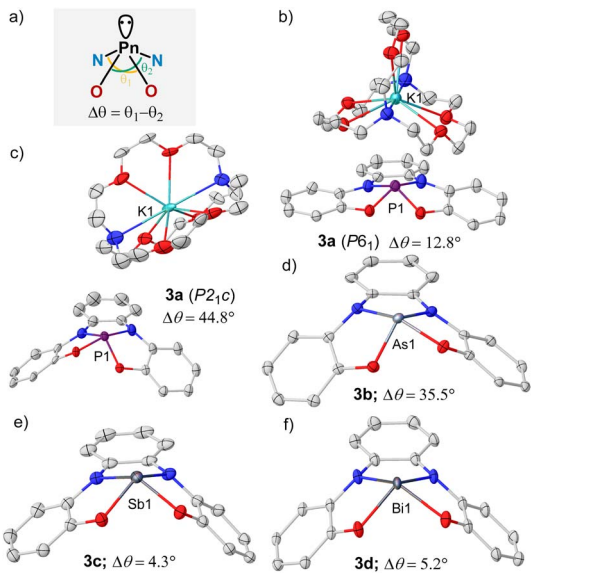


Fig. 1 (a) Definition of *trans* basal angles $\theta$ around the pnictogen; (b–f) X-ray solid-state structures of **3a–d**. Ellipsoids are shown at the 50% probability level. Hydrogens, cations (except for **3a**), *tert*-butyl groups and solvent molecules omitted for clarity.

depending of packing effects. Thus, when the potassium cation in phosphoranide **3a** is captured with 18-crown-6 ether, the P-atom adopts a perfect square pyramidal geometry and features a short P1–K1 contact (3.5899(12) Å) as reported by Dobrovetsky.[18]

Among the 10-Pn-4 anions, **3d** is particularly intriguing. While its solid-state structure definitely shows a pyramidal Bi(III) atom, another minimum (**3d′**) lying only 4.0 kcal mol$^{-1}$ higher in energy and characterized by a square planar geometry around the Bi-center has been found using DFT calculations at the PBE0-D3(BJ)/def2-TZVP(PCM)//TPSS-D3(BJ)/def2-TZVP level of theory (Fig. 2 and ESI†).[19] We assign the weak absorption centred at 980 nm in the UV-Vis spectrum of **3d** to traces of conformer **3d′** present in solution (see Fig. S15†). In **3d′**, a formally vacant 6p-orbital at Bi is available for mixing with the π-system of the redox active ligand making the assignation of the oxidation state of Bi not straightforward; in fact, the electronic structure of **3d′** is reminiscent to that of a Bi(I)-complex.[20] Similar triamide-Bi complexes have been described as Bi(I)/Bi(III) "redox-confused" for this reason.[21] This ill-defined situation motivated us to further evaluate the electronic structure in **3d′** by analyzing the effective fragment orbitals (EFOs)[22] and resulting effective oxidation states.[23]

In the experimentally observed pyramidal structure **3d**, the bismuth is undoubtedly in an oxidation state of +3 surrounded by a tetraanionic bis(amidophenolate) framework. The reliability index ($R$(%)) that quantifies how close the overall oxidation state assignment and the actual electronic structure of a molecule are, rises to 98.2% in this case. Yet, in **3d′** two electronic states are conceivable (Fig. 2b and c), which can be classified as Robin–Day Class III electromers.[24] According to EOS, the Bi(III) assignment persists as the most appropriate description, although with a lower reliability index ($R$(%) = 71.9).[25] The alternative description of **3d′** as a Bi(I) center within a dianionic tetradentate scaffold can be artificially produced within the EOS framework by switching the formal occupation of the last occupied and first unoccupied EFOs, yielding a non-aufbau electronic assignment with $R$(%) = 28.1.

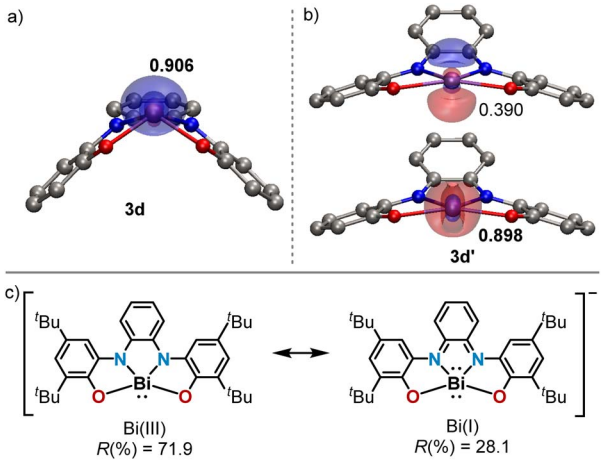


Fig. 2 (a and b) Optimized structures of **3d** and **3d′**, respectively, at the PBE0-D3(BJ)/def2-TZVP(PCM)//TPSS-D3(BJ)/def2-TZVP level of theory including the most relevant effective fragment orbitals (EFOs). Occupation values provided for each EFO, marked in bold the formally occupied. (c) Possible resonance structures of **3d′** including their associated EOS reliability index.

## Synthesis and characterization of Pn[CpFe(CO)$_2$] complexes

After the initial hints about possible electron redistribution from the surrounding framework to the pnictogen, we envisioned that this process might be fostered using Lewis acid coordination as a trigger. The cyclopentadienyliron(II) dicarbonyl cation was chosen for this task since it serves as probe for both IR and Mössbauer spectroscopy (Scheme 3).[26]

Phosphoranide **3a** was found to readily substitute the iodide in CpFe(CO)$_2$I upon mixture of the reagents in THF; however, the heavier homologues **3b–d** only coordinate the Fe-center when the more reactive [CpFe(thf)(CO)$_2$]BF$_4$ was employed. All compounds were obtained in moderate to good yields as air sensitive solids. Crystallization from MeCN solutions delivered monocrystals of sufficient quality for single-crystal X-ray diffraction analysis and the obtained solid-state structures confirm the coordination of **3a–d** to Fe through the central pnictogen donor atom, forming **4a–c** and **4d′**. As expected, the Pn–Fe bond lengths progressively increase when moving down in the pnictogen group, and are in agreement with the reported values for Pn–Fe bonds featuring pnictogen-based X-type ligands Fig. 3a–d.[26a,27]

The geometries of complexes **4a–c** are very similar, only an increased pyramidalization degree is found for the pnictogen atom when descending in the group (sum of basal angles: 340.4° (**4a**); 335.7° (**4b**, average value); 326.9° (**4c**)). The bismuth congener, however, opposes this trend having the Bi atom perfectly embedded in the plane defined by the oxygen and nitrogen donors (sum of basal angles around Bi = 360.1(11)°). This indicates that, unlike for the lighter pnictogens, in **4d′** the Bi(6p) orbital is used to form the bond with Fe while the Bi atom retains its 6s inert pair; hence, the 12-Bi-5 electromeric state is favored over the 10-Pn-5 observed for **4a–c**.

Closer comparison of the bond lengths and geometries in **4a–c** and **4d′** reveals that the extra electron pair surrounding the Bi center stems from the bis(amidophenolate) scaffold. The diagnostic N1–C15 and N2–C20 bond lengths in **4d′** are significantly shortened when compared with those in **4c** (*ca.* −0.06 Å). Moreover, the alternating short and long C–C bond lengths throughout the central carbocycle in **4d′** further suggests the

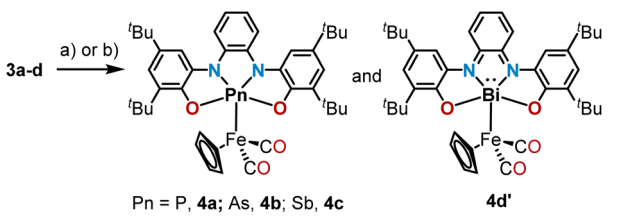


Scheme 3 Synthesis of 10-Pn-5 and 12-Pn-5 Fe-complexes. Reaction conditions: (a) CpFe(CO)$_2$I (1.00 equiv.), THF, rt, **4a** (64%).; (b) [CpFe(thf)(CO)$_2$]BF$_4$ (1.00 equiv.), DCM, −78 °C to rt, **4b** (47%), **4c** (72%), **4d′** (64%).

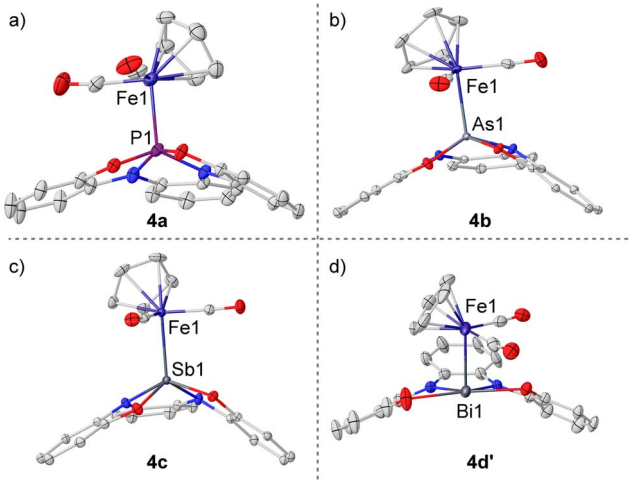


Fig. 3 (a) X-ray solid-state structures of **4a–c** and **4d′**. Ellipsoids are shown at the 50% probability level. Hydrogens, cations, *tert*-butyl groups and solvent molecules omitted for clarity. Selected bond lengths (Å): **4a**, P1–Fe1 2.2540(4); **4b**, As1–Fe1 2.3071(3); **4c**, Sb1–Fe1 2.4507(3); **4d′**, Bi1–Fe1 2.6052(13).

partial dearomatization of this ring and a considerable contribution of a bis(imine) structure for the ligand in **4d′**. The bond lengths in the amidophenolate side-arms were also inspected using the metrical oxidation state (MOS) method reported by Brown.[28] The values obtained for **4c** (−2.02(6), −1.98(6)) are the typical for completely reduced amidophenolate moieties, while in **4d′** the MOS's are significantly increased (−0.99(14), −1.12(10)) revealing a substantial (imino)semiquinone character (Fig. 4).

In order to scrutinize electronic changes at the iron center, all four iron complexes were further analyzed by $^{57}$Fe Mössbauer spectroscopy (Fig. 5). The obtained parameters for the isomeric shift $\delta$ are very similar throughout the series (**4a:** 0.08 mm s$^{-1}$, **4b:** 0.12 mm s$^{-1}$, **4c:** 0.14 mm s$^{-1}$, **4d′:** 0.14 mm s$^{-1}$), indicating a similar s-electron density at the iron nuclei and suggesting that differences in Fe(s) character mixing into σ(Fe–Pn) orbitals and in Fe(d) orbital populations are either negligible, or that their effects are compensating. The $\delta$ values agree with those of previous examples of Fp-complexes with X-type ligands such as [CpFe$^{II}$(CO)$_2$X] (X = Me, Cl, Br, I or P(O)(OMe)$_2$),[26b,c] but also with those found in formal CpFe$^0$(CO)$_2$ compounds.[26d] The quadrupole splitting $\Delta E_Q$ is basically equal for the structurally similar complexes **4a–c**, reflecting a similar local geometry and electric field gradient at Fe. The $\Delta E_Q$ value decreases by around 0.1 mm s$^{-1}$ for the bismuth congener **4d′**, which might be related to the altered geometry of the bis(amidophenolato) bismuth fragment; however, no clear relation to bond distances or angles around the Fe-center was found.

More precise information on the electronic situation at the Fe-center was obtained from infrared spectroscopic measurements. The carbonyl regions of the IR spectra of **4a–c** and **4d′** are depicted in Fig. 6. According to these spectra, the carbonyl stretching bands are higher in energy when descending in the period from **4a** to **4c**. This suggests lower donor ability for the heavier pnictogens as consequence of a more internal electron pair. However, **4d′** breaks this trend and exhibits the least energetic stretching bands of all the series ($\tilde{\nu}_{sym}$ = 2004, $\tilde{\nu}_{asym}$ = 1962 cm$^{-1}$), which are indicative of the strongest donor ability

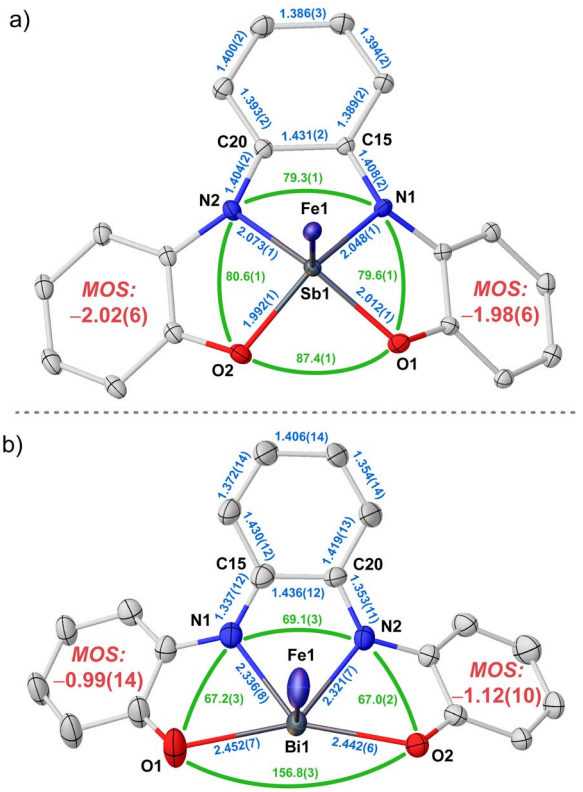


Fig. 4 Comparative analysis of the bond lengths, angles and metrical oxidation states in **4c** (a) and **4d′** (b).

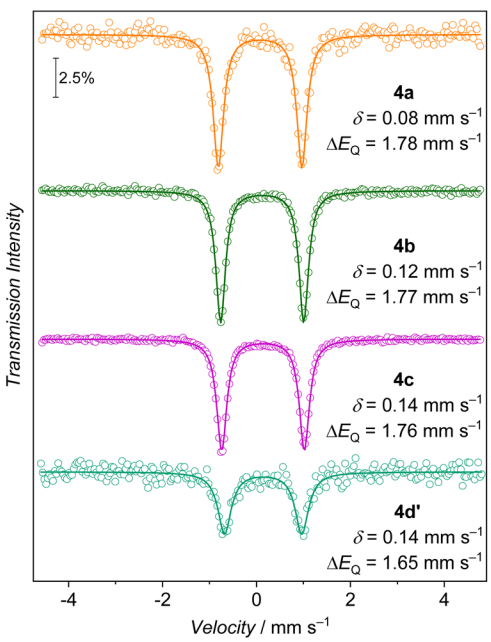


Fig. 5 Zero-field $^{57}$Fe Mössbauer spectra of **4a–c** and **4d′** at 80 K. Isomer shifts are given relative to α-Fe at 298 K.

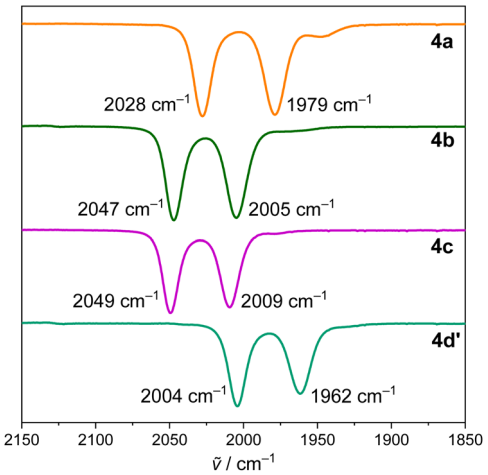


Fig. 6 FT-IR spectra of **4a–c** and **4d′** in DCM solution.

of the bis(amidophenolate)Bi moiety and the weakest polarization of the iron–bismuth bond along the pnictogen series.[27b]

Compounds **4a–c** and **4d′** were further analyzed by UV/vis spectroscopy (Fig. 7). The spectra of **4a–c** in DCM are quite similar at first glance and are dominated by intense transitions at around 300 nm. Interestingly, a broad band in the visible region was present with distinct maxima at 556 nm (**4b**) and 622 nm (**4c**), this band is also observed in the spectrum of **4a** as a shoulder ranging from *ca.* 400 to 500 nm. Time-dependent DFT calculations aided in the assignment of this band as a HOMO → LUMO transition (see ESI†). The HOMOs of **4a–c** are in all cases a π-orbital mainly localized at the bis(amidophenolate) unit. LUMOs are mostly distributed along the Pn–Fe bond axes and have σ*(Pn–Fe) character (see the ESI). Thus, these transitions can be described as charge-transfer bands and the redshift observed from P to Sb is explained by the LUMO energy decrease along the series, which aligns with the electron density reduction at the Fe-center (detected by IR spectroscopy).

The spectrum of **4d′** is starkly different and its most diagnostic feature is the strong low-energy absorption band with a maximum at 1090 nm (22 900 $M^{-1}$ $cm^{-1}$). This band corresponds to a π→π* transition that has been observed in numerous two electron-oxidized derivatives of the bis(amidophenolate) ligand **1**.[14,29] Thereby, the spectral data nicely

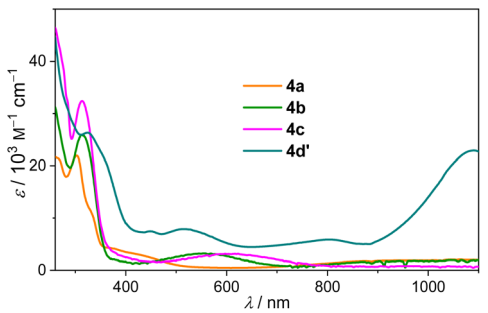


Fig. 7 Electronic absorption spectra of **4a–c** and **4d′**.

corroborate the change of electronic structure as a result of the 10-Pn-5/12-Pn-5 electromerism.

## Iron–pnictogen bonding and oxidation state determination

In order to elucidate the nature of the pnictogen–iron bonding interactions, we evaluated the electronic structure and performed chemical bonding analysis on the experimentally synthesized systems **4a–c** and **4d′**, together with the computationally modelled electromers **4b′** and **4c′**, in which the Pn-atom depicts square planar geometry and the ligand is formally oxidized. The computed relative Gibbs free energies agree with the experimentally observed electromeric forms. In particular, **4b** is more stable than **4b′** by 24.0 kcal $mol^{-1}$; for **4c** and **4c′** the energy difference decreases to 8.2 kcal $mol^{-1}$. All attempts to find the conceivable structures **4a′** and **4d** as local minima in the potential energy surface failed. Notably, our calculations predict the lowest electronic state of **4c′** and **4d′** to be an open-shell singlet.

The topology of the computed electron densities was investigated within the quantum theory of atoms in molecules (QTAIM) framework to shed light on the Pn–Fe bonding situation.[30] As illustrative example, Fig. 8 shows the contour maps of the electron density Laplacian for As-electromers **4b** and **4b′**. The Fe–As bond critical point lies in a region of charge depletion for both electromers, a common feature for bonding

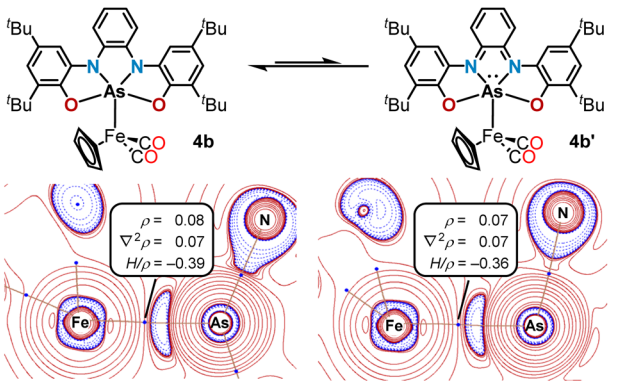


Fig. 8 Contour plots of the Laplacian of the electron density ∇2ρ for **4b** and **4b′** calculated at the PBE0-D3(BJ)/def2-TZVP(PCM)//TPSS-D3(BJ)/def2-TZVP level of theory. Blue: charge accumulation ($\nabla^2\rho$ < 0). Red: charge depletion ($\nabla^2\rho$ > 0).

Table 1 Selected QTAIM data: electron density (*ρ*), Laplacian of the electron density ($\nabla^2\rho$) and relative total energy density ($H/\rho$) at the pnictogen–iron bond critical point, pnictogen–iron delocalization index (DI) and bond distance (*d*)

| | *ρ*/a.u. | $\nabla^2\rho$/a.u. | $H/\rho$/a.u. | DI | *d*/Å |
|---|---|---|---|---|---|
| **4a** | 0.094 | 0.066 | −0.40 | 0.72 | 2.286 |
| **4b** | 0.083 | 0.073 | −0.39 | 0.70 | 2.355 |
| **4c** | 0.069 | 0.056 | −0.35 | 0.68 | 2.506 |
| **4b′** | 0.073 | 0.070 | −0.36 | 0.64 | 2.407 |
| **4c′** | 0.062 | 0.034 | −0.32 | 0.66 | 2.585 |
| **4d′** | 0.057 | 0.043 | −0.28 | 0.69 | 2.665 |

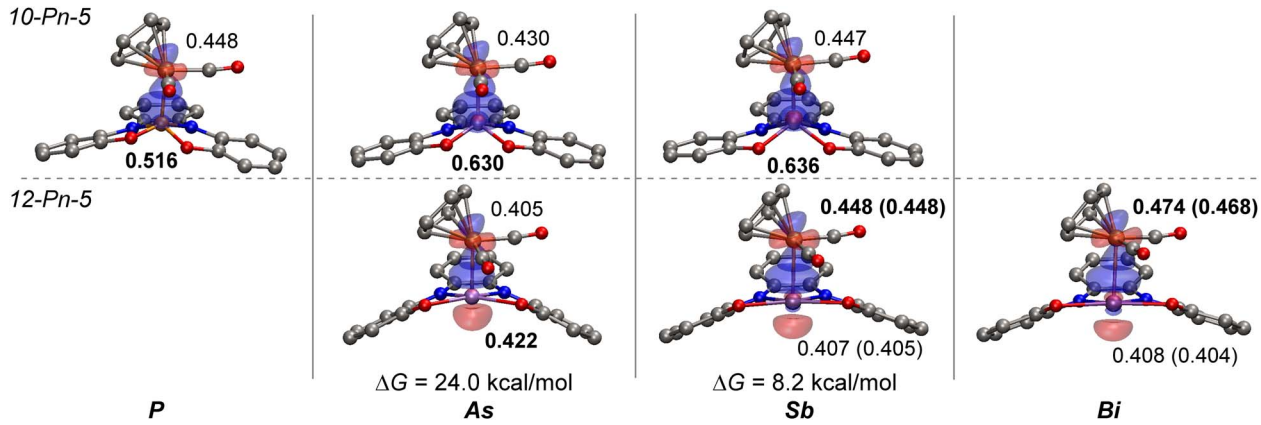


Fig. 9 Frontier EFOs and their associated occupation values for the reduced and oxidized species studied. For open-shell systems, beta EFO occupancies are reported in parentheses. Marked in bold are the EFOs formally occupied according to the EOS analysis.

between atoms having more than three atomic shells.[31] For these relatively heavy atoms, Bader's classification of bonding interactions based on the sign of the Laplacian cannot simply be extrapolated,[32] and other parameters need to be considered.[31] Thus, structures **4b** and **4b′** exhibit negative relative energy densities $H/\rho$ at the bond critical point, fulfilling the Cremer–Kraka criteria for covalent bonding (Table 1).[33]

The electron density at the bond critical point decreases quite uniformly throughout the **4a–c** series as result of the longer bond distances and the more diffuse nature of the electron density for the heavier pnictogens. The calculated delocalization indices (DI) are in agreement with the formulation of covalent Pn–Fe single bonds for all compounds; yet, an intriguing trend is revealed. For the 10-Pn-5 compounds **4a–c**, the DI gradually decreases for the heavier pnictogens, while the opposite trend is observed for the 12-Pn-5 isomers **4b′–d′**. Since the DI is directly related with the extent of delocalization of electron pairs between two atomic basins[31] and has been used to quantify covalent bond orders,[32] it seems that the covalency of the Pn–Fe bond reaches two maxima, one for the lighter 10-P-5 system in **4a** and a second one for the heavier 12-Bi-5 electromer in **4d′**.

The shape and occupation values of the EFOs involved in the σ-type Pn–Fe bond are shown in Fig. 9. The EFO/EOS analysis was performed for all systems considering each ligand coordinated at the Fe and Pn atoms as fragments. This allows the disentangling of the Fe–Pn interaction from the rest of the ligands. For the pyramidal-shaped species **4a–c** (Fig. 9 top), the Fe–Pn bond is formed by a d-type EFO sitting on Fe, with the s-type EFO from the pnictogen. The latter shows an increase of occupation value from 0.516 (**4a**) to 0.630 (**4a**) and in 0.636 (**4c**). Hence, the heavier the central element, the more polarized the Fe–Pn bond towards Pn. This is well in agreement with the lower tendency of the higher pnictogens to involve their s-electrons in bonding, and also supported by our IR data. The difference in occupation between these two EFOs also hints at the degree of covalency of the bond. The lower the difference is, the greater the covalent character of the bond. Therefore, the Fe–P (**4a**) bond is more covalent than both Fe–As (**4b**) and Fe–Sb (**4c**), agreeing with the topological analysis of the electron densities (see ESI†).

For the 12-Pn-5 species **4b′–d′** (Fig. 9 bottom), the Fe–Pn bond is formed by a d-type Fe EFO interacting with a properly oriented p-type EFO from the pnictogen, which is formally occupied as consequence of the bis(amidophenolate) oxidation. Interestingly, for this species the pnictogen s-type EFO does not participate in bonding to the Fe.

Finally, the oxidation states of **4a–c** and **4d′** have been calculated. In **4a–c**, the Cp, CO and ONNO scaffolds are characterized by oxidation states −1, 0 and −4, respectively. For the central Pn an oxidation state +3 is assigned, and subsequently, the Fe atom is in oxidation state +2. This electronic distribution is more evident for As and Sb ($R(\%) = 70.0$ and 68.9, respectively); yet, for **4a** the reliability index is significantly reduced ($R(\%) = 56.9$) due to the large covalency of the P–Fe bond. The same analysis in Bi complex **4d′** assigns an oxidation state of −2 to the ONNO ligand, +3 to Bi, and 0 to Fe, instead of the more intuitive Bi(I)/Fe(II) oxidation states. It should be noted that this solution shows a lower reliability index ($R(\%) = 56.5$), denoting how difficult the electron pair assignment in the Bi–Fe interaction is (see Fig. 9). This discrepancy suggests that in **4d′** the planarized Bi-atom simply serves as transmission belt to transfer electron density for the bis(amidophenolate) ligand to the Fe-center.

## Conclusions

A series of geometrically constrained bis(amidophenolate)-supported pnictoranide anions has been synthesized and structurally characterized. An Effective Oxidation State analysis of these anions unambiguously assigns an oxidation state +3 to the P-, As- and Sb-complexes, while it suggests some +1 character to the Bi-derivative due to the efficient mixture of the Bi(6p) orbital with the π-system of the redox-active supporting ligand. Coordination of these species to the $[CpFe(CO)_2]^+$ moiety was achieved. For the P-, As- and Sb-derivatives the pnictogen atom remains pyramidal but the Bi-atom planarizes. The Effective Oxidation State analysis of that complex still assigns an oxidation state +3 to Bi while the Fe atom is reduced

from +2 to 0. The mixture of the Bi(6p)-orbital with the π-system of the bis(amidophenolate) ligand in the square planar geometry, and the efficient electronic donation from that orbital to the Fe-center explain this non-intuitive situation.

## Data availability

All data associated with this article are available from the ESI.†

## Author contributions

S. B. H. K. and M. A. conceived the project and designed the experiments. S. B. H. K. and J. F. K. performed the experiments and analysed the results. S. B. H. K. and M. G. carried out the computational studies. C. G. performed the X-ray crystallographic analysis. I. B. and F. M. collected and analysed the Mössbauer spectroscopy data. All authors discussed the results, and S. B. H. K., M. G. and M. A. prepared the manuscript.

## Conflicts of interest

There are no conflicts to declare.

## Acknowledgements

Financial support from the DFG through the projects INST 186/1237-1, INST 186/1318-1 and INST 186/1324-1 is gratefully acknowledged. We also thank the NMR and MS services, as well as the analytical laboratory at the Faculty of Chemistry (University of Göttingen) for technical assistance, and Prof. Ricardo A. Mata (University of Göttingen) for insightful discussions. I. B. is grateful for a Kekulé PhD fellowship from the Fonds der Chemischen Industrie (FCI). M. G. acknowledges support by the DFG – 217133147/SFB 1073.

## Notes and references

1 (*a*) M. A. Dunstan and K. S. Pedersen, *Chem. Commun.*, 2025, **61**, 627–638; (*b*) J. R. Reimers and L. K. McKemmish, in *Mixed Valence Systems:Fundamentals, Synthesis, Electron Transfer, and Applications*, ed. Y.-W. Zhong, C. Y. Liu and J. R. Reimers, Wiley-VCH GmbH, Weinheim, 2023, ch. 2; (*c*) T. Tezgerevska, K. G. Alley and C. Boskovic, *Coord. Chem. Rev.*, 2014, **268**, 23–40; (*d*) E. Evangelio and D. Ruiz-Molina, *Eur. J. Inorg. Chem.*, 2005, **15**, 2957–2971; (*e*) P. Gütlich and A. Dei, *Angew. Chem., Int. Ed.*, 1997, **36**, 2734–2736; (*f*) L. W. Jones, *Science*, 1917, **46**, 493–502.

2 (*a*) K. S. Kumar and M. Ruben, *Coord. Chem. Rev.*, 2017, **346**, 176–205; (*b*) M. D. Manrique-Juarez, S. Rat, L. Salmon, G. Molnar, C. M. Quintero, L. Nicu, H. J. Shepherd and A. Bousseksou, *Coord. Chem. Rev.*, 2016, **308**, 395–408; (*c*) O. Sato, J. Tao and Y.-Z. Zhang, *Angew. Chem., Int. Ed.*, 2007, **46**, 2152–2187; (*d*) J.-F. Létard, P. Guionneau and L. Goux-Capes, *Top. Curr. Chem.*, 2004, **235**, 221–249; (*e*) O. Kahn and C. J. Martinez, *Science*, 1998, **279**, 44–48.

3 Selected examples: (*a*) J. T. Janetzki, D. S. Brown, F. Daumann, I. H. Ismail, R. W. Gable, M. A. Hay, R. J. Mulder, A. A. Starikova, B. Weber, M. J. Giansiracusa and C. Boskovic, *Chem. Sci.*, 2025, **16**, 5857–5871; (*b*) D. A. Lukina, A. A. Skatova, R. V. Rumyntcev, S. V. Demeshko, F. Meyer and I. L. Fedushkin, *Dalton Trans.*, 2024, **53**, 8850–8856; (*c*) C. Metzger, R. Dolai, S. Reh, H. Kelm, M. Schmitz, B. Oelkers, M. Sawall, K. Neymeyr and H.-J. Krüger, *Chem.–Eur. J.*, 2023, **29**, e202300091; (*d*) K. K. C., T. Woods and L. Olshansky, *Angew. Chem., Int. Ed.*, 2023, **62**, e202311790; (*e*) C. Lecourt, Y. Izumi, L. Khrouz, F. Toche, R. Chiriac, N. Bélanger-Desmarais, C. Reber, O. Fabelo, K. Inoue, C. Desroches and D. Luneau, *Dalton Trans.*, 2020, **49**, 15646–156632; (*f*) G. K. Gransbury, B. N. Livesay, J. T. Janetzki, M. A. Hay, R. W. Gable, M. P. Shores, A. Starikova and C. Boskovice, *J. Am. Chem. Soc.*, 2020, **142**, 10692–10704; (*g*) J. Chen, Y. Sekine, Y. Komatsumaru, S. Hayami and H. Miyasaka, *Angew. Chem., Int. Ed.*, 2018, **57**, 12043–12047.

4 Selected examples: (*a*) A. Summers, F. Z. M. Zahir, G. F. Turner, M. A. Hay, A. Riboldi-Tunnicliffe, R. l. Williamson, S. Bird, L. Goerigk, C. Boskovic and S. A. Moggach, *Nat. Commun.*, 2024, **15**, 8922; (*b*) A. Caneschi, A. Die, F. Fabrizi de Biani, P. Gütlich, V. Ksenofontov, G. Levchenko, A. Hoefer and F. Renz, *Chem.–Eur. J.*, 2001, **7**, 3926–3930; (*c*) C. Roux, D. M. Adams, J. P. Itié, A. Polian, D. N. Hendrickson and M. Verdaguer, *Inorg. Chem.*, 1996, **35**, 2846–2852.

5 Selected examples: (*a*) W.-H. Xu, Y.-B. Huang, W.-W. Zheng, S.-Q. Su, S. Kanegawa, S.-Q. Wu and O. Sato, *Chem. Sci.*, 2024, **53**, 2512–2516; (*b*) A. Witt, F. W. Heinemann and M. M. Khusniyarov, *Chem. Sci.*, 2015, **6**, 4599–4609; (*c*) O. Sato, A. Cui, R. Matsuda, J. Tao and S. Hayami, *Acc. Chem. Res.*, 2007, **40**, 361–369.

6 Selected examples: (*a*) N. Ansmann, M. Kerscher and L. Greb, *Angew. Chem., Int. Ed.*, 2025, **64**, e202417581; (*b*) A. Witt, F. W. Heinemann, S. Sproules and M. M. Khusniyarov, *Chem.–Eur. J.*, 2014, **20**, 11149–11162; (*c*) T. Storr, E. C. Wasinger, R. C. Pratt and T. D. P. Stack, *Angew. Chem., Int. Ed.*, 2007, **46**, 5198–5201.

7 R. M. Buchanan and C. G. Pierpont, *J. Am. Chem. Soc.*, 1980, **102**, 4951–4957.

8 (*a*) S. B. H. Karnbrock and M. Alcarazo, *Chem.–Eur. J.*, 2024, **30**, e202302879; (*b*) L. Greb, *Eur. J. Inorg. Chem.*, 2022, **2022**, e202100871.

9 J. A. Cissell, T. P. Vaid and G. P. A. Yap, *J. Am. Chem. Soc.*, 2007, **129**, 7841–7847.

10 A. J. Arduengo, C. A. Stewart and F. Davidson, *J. Am. Chem. Soc.*, 1986, **108**, 322–323.

11 R. Yadav, X. Sun, R. Köppe, M. T. Gamer, F. Weigend and P. W. Roesky, *Angew. Chem., Int. Ed.*, 2022, **61**, e202211115.

12 (*a*) S. Yao, A. Kostenko, Y. Xiong, C. Lorent, A. Ruzicka and M. Driess, *Angew. Chem., Int. Ed.*, 2021, **60**, 14864–14868; (*b*) S. Yao, A. Kostenko, Y. Xiong, A. Ruzicka and M. Driess, *J. Am. Chem. Soc.*, 2020, **142**, 12608–12612.

13 M. G. Chegerev, A. V. Piskunov, A. A. Starikova, S. P. Kubrin, G. K. Fukin, V. K. Cherkasov and G. A. Abakumov, *Eur. J. Inorg. Chem.*, 2018, **2018**, 1087–1092.

14 S. B. H. Karnbrock, J. F. Köster, C. Golz, R. A. Mata and M. Alcarazo, *Angew. Chem., Int. Ed.*, 2025, e202501439.
15 M. Schorpp, R. Yadav, D. Roth and L. Greb, *Angew. Chem., Int. Ed.*, 2022, **61**, e202207963.
16 (*a*) S. B. H. Karnbrock, C. Golz, R. A. Mata and M. Alcarazo, *Angew. Chem., Int. Ed.*, 2022, **61**, e202207450; (*b*) S. B. H. Karnbrock, C. Golz and M. Alcarazo, *Chem. Commun.*, 2024, **60**, 6745–6748.
17 (*a*) M. Mantina, A. C. Chamberlin, R. Valero, C. J. Cramer and D. G. Truhlar, *J. Phys. Chem. A*, 2009, **113**, 5806–5812; (*b*) A. Bondi, *J. Phys. Chem.*, 1964, **68**, 441–451.
18 S. Volodarsky, I. Malahov, D. Bawari, M. Diab, N. Malik, B. Tumanskii and R. Dobrovetsky, *Chem. Sci.*, 2022, **13**, 5957–5963.
19 (*a*) C. Adamo and V. Barone, *J. Chem. Phys.*, 1999, **110**, 6158; (*b*) S. Grimme, S. Ehrlich and L. Goerigk, *J. Comput. Chem.*, 2011, **32**, 1456; (*c*) G. Scalmani and M. J. Frisch, *J. Chem. Phys.*, 2010, **132**, 114110; (*d*) F. Weigend and R. Ahlrichs, *Phys. Chem. Chem. Phys.*, 2005, **7**, 3297; (*e*) J. M. Tao, J. P. Perdew, V. N. Staroverov and G. E. Scuseria, *Phys. Rev. Lett.*, 2003, **91**, 146401.
20 (*a*) M. Kořenková, V. Kremláček, M. Erben, R. Jirásko, F. De Proft, J. Turek, R. Jambor, A. Růžička, I. Císařova and L. Dostál, *Dalton Trans.*, 2018, **47**, 14503–14514; (*b*) I. Vránová, T. Dušková, M. Erben, R. Jambor, A. Růžička and L. Dostál, *J. Organomet. Chem.*, 2018, **863**, 15–20; (*c*) M. Kořenková, V. Kremláček, M. Erben, R. Jambor, Z. Růžičková and L. Dostál, *J. Organomet. Chem.*, 2017, **845**, 49–54; (*d*) I. Vránová, V. Kremláček, M. Erben, J. Tzrek, R. Jambor, A. Růžička, M. Alonso and L. Dostál, *Dalton Trans.*, 2017, **46**, 3556–3568.
21 (*a*) P. Coburger, A. G. Buzanich, F. Emmerling and J. Abbenseth, *Chem. Sci.*, 2024, **15**, 6036–6043; (*b*) M. B. Kindervater, K. M. Marczenko, U. Werner-Zwanziger and S. S. Chitnis, *Angew. Chem., Int. Ed.*, 2019, **58**, 7850–7855; (*c*) K. M. Marczenko, J. A. Zurakowski, M. B. Kindervater, S. Jee, T. Hynes, N. Roberts, S. Park, U. Werner-Zwanziger, M. Lumsden, D. N. Langelaan and S. S. Chitnis, *Chem.–Eur. J.*, 2019, **25**, 16414–16424.
22 E. Ramos-Cordoba, P. Salvador and I. Mayer, *J. Chem. Phys.*, 2013, **138**, 214107.
23 (*a*) E. Ramos-Cordoba, V. Postils and P. Salvador, *J. Chem. Theory Comput.*, 2015, **11**, 1501–1508; (*b*) P. Salvador, E. Ramos-Cordoba, M. Montilla, L. Pujal and M. Gimferrer, *J. Chem. Phys.*, 2024, **160**, 172502; (*c*) In the EOS framework, the difference in occupation between the last occupied (LO) and first unoccupied (FU) EFOs is used to evaluate the reliability of the assignment ($R$(%) index) as $R(\%) = 100(\lambda_{LO} - \lambda_{FU} + 1/2)$. By definition, when the difference between occupations of the frontier EFOs exceeds half an electron, the oxidation state (OS) assignment is considered indisputable ($R$(%) = 100). An $R$% value of 50 implies that the two possible effective electronic configurations are equally plausible.
24 M. B. Robin and P. Day, in *Advances in Inorganic Chemistry and Radiochemistry*, ed. H. J. Emeléus and A. G. Sharpe, Academic Press, 1968, vol. 10, 247–422.
25 The same analysis for the T-shape planar triamide bismuthine reported by Chitnis (ref. 21*b*M. Gimferrer, S. Danés, D. M. Andrada and P. Salvador, *Inorg. Chem.*, 2021, **60**, 17657) suggest a Bi(III) center and a formal trianionic NNN ligand with $R(\%) = 65.0$.
26 (*a*) K. Kubo, H. Nakazawa, T. Mizuta and K. Miyoshi, *Organometallics*, 1998, **17**, 3522–3531; (*b*) H. Nakazawa, S. Ichimura, Y. Nishihara, K. Miyoshi, S. Nakashima and H. Sakai, *Organometallics*, 1998, **17**, 5061–5067; (*c*) M. K. Karunananda, F. X. Vazquez, E. E. Alp, W. Bi, S. Chattopadhyay, T. Shibata and N. P. Mankad, *Dalton Trans.*, 2014, **43**, 13661; (*d*) D. Kim, D. W. N. Wilson, M. S. Fataftah, B. W. Mercado and P. L. Holland, *Chem.–Eur. J.*, 2022, **28**, e202104431.
27 (*a*) J. Ramler, F. Geist, C. Mihm, L. Lubczyk, S. Reith, C. Herok, F. Fantuzzi and C. Lichtenberg, *Chem.–Eur. J.*, 2025, **31**, e202403253; (*b*) J. Ramler and C. Lichtenberg, *Dalton Trans.*, 2021, **50**, 7120–7138; (*c*) J. Ramler, I. Krummenacher and C. Lichtenberg, *Angew. Chem., Int. Ed.*, 2019, **58**, 12924–12929; (*d*) K. Wójcik, P. Ecorchard, D. Schaarschmidt, T. Rüffer, H. Lang and M. Mehring, *Z. Anorg. Allg. Chem.*, 2012, **638**, 1723–1730; (*e*) Y. Yamamoto, M. Okazaki, Y. Wakisaka and K. Akiba, *Organometallics*, 1995, **14**, 3364–3369; (*f*) S. K. Chopra and J. C. Martin, *Heteroat. Chem.*, 1991, **2**, 71–79; (*g*) M. Wieber, D. Wirth and C. Burschka, *Z. Naturforsch., B: J. Chem. Sci.*, 1985, **40**, 258–262.
28 S. N. Brown, *Inorg. Chem.*, 2012, **51**, 1251–1260.
29 (*a*) J. Underhill, E. S. Yang, T. Schmidt-Räntsch, W. K. Myers, J. M. Goicoechea and J. Abbenseth, *Chem.–Eur. J.*, 2023, **29**, e202203266; (*b*) A. J. Pistner, H. W. Moon, A. Silakov, H. P. Yennawar and A. T. Radosevich, *Inorg. Chem.*, 2017, **56**, 8661–8668; (*c*) F. Lu, R. A. Zarkesh and A. F. Heyduk, *Eur. J. Inorg. Chem.*, 2012, **2012**, 467–470; (*d*) K. J. Blackmore, N. Lal, J. W. Ziller and A. F. Heyduk, *Eur. J. Inorg. Chem.*, 2009, **2009**, 735–743; (*e*) P. Chaudhuri, M. Hess, J. Müller, K. Hildenbrand, E. Bill, T. Weyhermüller and K. Wieghardt, *J. Am. Chem. Soc.*, 1999, **121**, 9599–9610.
30 R. F. W. Bader, *Atoms in molecules. A quantum theory*, Clarendon Press, Oxford, 2003.
31 C. Gatti, *Z. Kristallogr. – Cryst. Mater.*, 2005, **220**, 399–457.
32 R. F. W. Bader and H. Essén, *J. Chem. Phys.*, 1984, **80**, 1943–1960.
33 D. Cremer and E. Kraka, *Angew Chem. Int. Ed. Engl.*, 1984, **23**, 627–628.